frontiers | Frontiers in Earth Science

ORIGINAL RESEARCH
published: 27 April 2022
doi: 10.3389/feart.2022.906987

Sequence Stratigraphy, Depositional Environment and Associated Lithofacies of Lacustrine Shale: A Case From the Upper Fourth Member of Shahejie Formation, Dongying Depression, Bohai Bay Basin

Guiang Li[1], *Chengyan Lin*[1,2]*, *Chunmei Dong*[1,2], *Pengjie Ma*[1,2]*, *Xinyu Du*[1], *Long Jiang*[3] and *Feng Guo*[4]

[1]School of Geosciences, China University of Petroleum (East China), Qingdao, China, [2]Reservoir Geology Key Laboratory of Shandong Province (East China), Qingdao, China, [3]Geological Scientific Research Institute of Shengli Oilfield, SINOPEC, Dongying, China, [4]Geological Scientific Research Institute of Liaohe Oilfield, CNPC, Panji, China

OPEN ACCESS

Edited by:
Kun Zhang,
Southwest Petroleum University, China

Reviewed by:
Zhongxiang Zhao,
Yangtze University, China
Shansi Tian,
Northeast Petroleum University, China
Zheng Cao,
Chongqing University of Science and Technology, China

***Correspondence:**
Chengyan Lin
lincy@upc.edu.cn
Pengjie Ma
mapengjie1989@upc.edu.cn

Specialty section:
This article was submitted to Economic Geology, a section of the journal Frontiers in Earth Science

Received: 29 March 2022
Accepted: 06 April 2022
Published: 27 April 2022

Citation:
Li G, Lin C, Dong C, Ma P, Du X, Jiang L and Guo F (2022) Sequence Stratigraphy, Depositional Environment and Associated Lithofacies of Lacustrine Shale: A Case From the Upper Fourth Member of Shahejie Formation, Dongying Depression, Bohai Bay Basin. Front. Earth Sci. 10:906987. doi: 10.3389/feart.2022.906987

The lithofacies assemblages in the lacustrine shale of the Shahejie Formation in the Dongying Depression have different compositions due to the complex depositional climate, lake water conditions, and sediment supply. Hence, the lithofacies types and depositional conditions were analyzed based on parasequence division and lithofacies classification. According to gamma ray integrated prediction error filter analysis (INPEFA), handheld x-ray fluorescence (XRF) measurements, mineral composition, total organic carbon (TOC) content, and sedimentary structures, six parasequences (P1–P6 from bottom to top) were identified, and seven lithofacies are recognized: (1) organic-poor thin-bedded calcareous mudstone, (2) organic-poor laminated calcareous mudstone, (3) intermediate-organic laminated calcareous mudstone, (4) organic-rich laminated calcareous mudstone, (5) organic-rich calcareous shale, (6) organic-rich laminated carbonate-bearing mudstone, and (7) laminated silty mudstone. When the climate became warm and wet, the water level of the lake increased with a decrease in salinity, and the corresponding lithofacies assemblages in the P1 to P2 parasequences gradually changed from organic-poor thin-bedded and laminated calcareous mudstone to intermediate-organic and organic-rich calcareous shale. When the climate became humid and warmer, resulting in an increasing water level and terrigenous input, the lithofacies assemblages in the P3–P4 parasequences changed from organic-rich calcareous shale and laminated carbonate-bearing mudstone to laminated silty mudstone and calcareous mudstone. At the end, the climate became slightly drier and cooler with a decrease in the water level, and the P5 and P6 parasequences were dominated by intermediate-organic and organic-poor laminated calcareous mudstones. Through elemental analysis and lithofacies observation, we found that the redox conditions of the water may have changed over time. Among the parasequences, the water column of the P2 parasequence was mainly stratified by salinity, that of the P4 parasequence was

mainly stratified by temperature, and that of the P3 parasequence was in transition. The synergistic effect of various factors played a key role in the enrichment of organic matter. This study highlights the depositional processes of the lithofacies assemblages in a lacustrine shale and contributes to the understanding of shale oil accumulation in lacustrine shale.

Keywords: lithofacies (assemblages), shale oil, sequence stratigraphy, Dongying depression, Bohai Bay basin

INTRODUCTION

With the successful development of marine shale gas in North America, shale oil and gas have become important unconventional energy sources (Hill et al., 2007; Jarvie et al., 2007; Aplin and Macquaker, 2011; Huang et al., 2020; Kang et al., 2019). Nevertheless, the evolution characteristics and distribution patterns of continental shale lithofacies types are still not well known due to their complexity and variability. Relatedly, the sedimentary environment and evolution process of continental shale remains unclear. In recent years, many scholars have performed studies on shale lithofacies division, sequence division, sedimentary environment analysis, diagenetic analysis and so on (Loucks and Ruppel, 2007; Rodriguez and Philp, 2010; Abouelresh and Slatt, 2012; Hao et al., 2013; Tian et al., 2021; Wu et al., 2019; Zeng et al., 2022). Although the sedimentary sequence and lithofacies development characteristics of shale are relatively complex, they are controlled by the evolution of the sedimentary environment, showing obvious segmented characteristics as a whole, and the lithofacies association changes regularly (Abouelresh and Slatt, 2012; Zhang et al., 2020a). Therefore, it is important to clarify the sedimentary evolution of mud shale to establish a high-precision sequence stratigraphic framework and then carry out the fine characterization of lithofacies types and analysis of lithofacies association characteristics.

For the division of continental shale lithofacies, the method involving four components and three endmembers has been mainly adopted at present. However, due to different angles of consideration, there are differences in lithofacies division in different research areas, as well as in the same research area (Dong et al., 2015; Liang et al., 2018a; Chen et al., 2008 Wu et al., 2017; Li et al., 2017; Zhang et al., 2018). It is considered the key to establish a reasonable lithofacies division scheme to consider the distribution pattern of rock components and carefully observe the characteristic differences in sedimentary structures through fine observation of core thin sections.

In addition, it is very difficult to study the stratigraphy of shale with a uniform structure deposited in relatively deep water, which prevents the application of traditional sequence stratigraphy in shale (Boulila et al., 2014). Some scholars have proposed solutions to the sequence division of shale, such as the gamma ray parasequences (GRP) method established by Slatt et al. (2008; Slatt et al., 2012), which is the most widely used method; this method mainly divides GRP cycles based on the superposition combination pattern of gamma ray (GR) curves. However, due to the frequent changes in GR curves, it is difficult to divide systems tracts and quasi-sequences and consider the existence of many subjective factors, leading to inconsistent results in the division of the same stratum and work area (Chen et al., 2008; Liang et al., 2018b). Therefore, finding a method that can objectively reflect the boundary of sequence division more intuitively and obviously is a difficult problem in the division of mud shale sequences.

The upper fourth member of the Eocene Shahejie Formation (Es4s) is a typical example of a Bohai Bay Basin lacustrine shale and is predominantly composed of carbonate, clay minerals and other mineral components that vary more widely than those of marine siliciclastic shales. Based on the division of a high-precision sequence stratigraphic framework, we clarify the characteristics of lithofacies assemblages at different stages, discuss the response of lithofacies to the evolution of the sedimentary environment, explore the development and distribution pattern of the dominant lithofacies assemblages and guide shale oil exploration (Yu et al., 2022; Gao, 2021; Wang et al., 2020).

GEOLOGICAL SETTING

The Dongying depression is located in the Jiyang Depression of the Bohai Bay Basin. It is a continental lake basin with an asymmetrical half-graben structure (**Figure 1**). The Dongying depression can be divided into four depressions: the Boxing depression, Niuzhuang depression, Lijin depression and Minfeng depression. The Dongying depression is approximately 90 km long from east to west and 65 km wide from north to south. The exploration area in the Dongying depression is approximately 5,760 km^2. The Paleogene strata are widely distributed; from bottom to top, they are the Kongdian Formation, Shahejie Formation, Dongying Formation, Guantao Formation and Minghuazhen Formation. The Shahejie Formation is subdivided into four members, Es4, Es3, Es2, and Es1 (from bottom to top). The Es4 strata are subdivided into the Upper Es4 (Es4s) interval and the Lower Es4 (Es4x) interval (**Figure 1**). The Es4s lake basin was in the prime stage of rift expansion, with strong subsidence and rapid expansion, forming a broad semideep to deep lake environment, and in this lake, lacustrine organic-rich black shale up to 200 m thick was deposited in the center of the lake basin.

DATA AND METHODS

Core and Thin Section Observations

Data for this study were collected from nearly 160 m of cores from Well NY1 in the Dongying depression, which penetrates the entirety of Es4s in the Shahejie Formation (**Figure 1**). Almost all publications about Es4s in the Shahejie Formation in the Dongying depression are based on this well. A total of 62 core

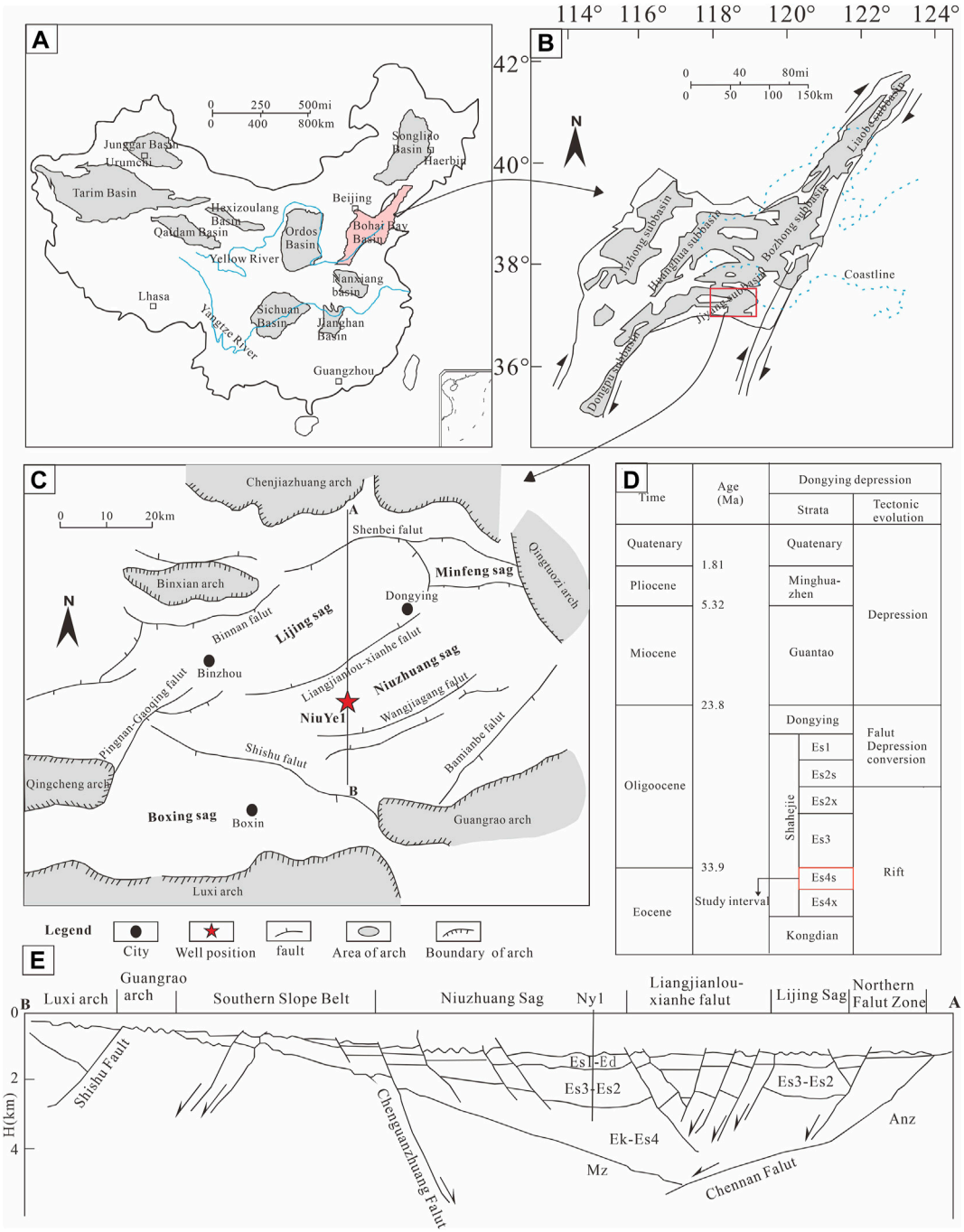

FIGURE 1 | Tectonic background map of the Dongying depression. **(A)** The geographical location of the Bohai Bay Basin in China. **(B)** The Dongying depression is located in the Bohai Bay Basin. **(C)** Structural distribution characteristics of the Dongying depression. **(D)** Stratigraphic column of the study area. **(E)** Structural section in the direction A–B, which is modified according to Liang et al. (2017).

samples were collected from the Es4s shale target interval for observation and testing. Thin sections with a thickness of 0.03 mm were prepared and observed under a polarizing Zeiss microscope (Axio Scope A1). These samples were also examined using a field emission scanning electron microscope (FE-SEM) from Carl Zeise (Supra 55).

Energy-Dispersive X-Ray Fluorescence Analysis

The elemental compositions (23 elements per sampling site) of core samples were measured on clean and smooth core surfaces using a Thermo Scientific Niton XL handheld energy-dispersive

X-ray fluorescence (ED-XRF) analyzer from the Reservoir Geology Key Laboratory of Shandong Province (East China), Qingdao, China, with a spatial resolution of 3–5 cm. The ED-XRF instrument has a built-in calibration system that measures in ppm and has been shown to provide a reliable first-hand view of the chemical stratigraphy of borehole cores (Rowe et al., 2012).

X-Ray Diffraction Analysis

X-ray diffraction (XRD) analysis was performed using an X'pert-Multipurpose diffractometer (MPD) from the Shengli Oilfield Geological Research Center, which consists of a copper butt, 30 kV pipe pressure, 40 mA conduit flow, and 2θ/min scanning speed.

Chemical Composition of Organic Matter

Total organic carbon (TOC) and hydrocarbon potential analyses were also performed on the samples. TOC was measured with a CS344 carbon and sulfur detector (Leco, United States), and free hydrocarbon analysis (e.g., S1; Mg HC/g rock) and kerogen cracking (S2; Mg HC/g rock) were performed using a Rock-Eval pyrolysis system (Rock-EVAL6). All analyses were carried out in the Shengli Oilfield Geological Research Center.

Integrated Prediction Error Filter Analysis

Spectral trend attribute analysis is a technique for identifying stratigraphic cycles by means of spectral analysis of logging or time series data (Nio et al., 2005). Based on the theory of cycle stratigraphy, the logging curve was converted into an integrated prediction error filter analysis (INPEFA) curve using digital signal processing, which reflects the hidden periods in the formation characteristic logging data. According to the principle of logging geology, different logging curves reflect different geological characteristics. Compared with other logging curves, the natural GR curve is the most sensitive to changes in mud content and is not sensitive to borehole conditions. It is a good index for analysis of the sedimentary environment. Thus, it is the most effective index to use for stratigraphic sequence research.

RESULTS

Mineralogical Characteristics

The Es4s shale are mainly composed of high percentages of calcite, clay minerals and quartz, while the contents of dolomite, pyrite, plagioclase and other minerals are low (Liang et al., 2018a). The mineral compositions of shale from Es4s in the Shahejie Formation in Well NY1 are shown in **Figure 2** and **Table 1**. The content of carbonate minerals is high in Es4s: the content of calcite is low and that of dolomite is high at the bottom of the section, and the content of calcite increases and that of dolomite decreases upward. Clay minerals and quartz are abundant in the range of 3,360–3,390 m, with average contents of 35 and 25%, respectively. The quartz content increases significantly at 3,390 m, with an average content of 33%. The feldspar content is low in Es4s, with an average content of 6%. The pyrite content is generally low, with an average content of 3%. The anhydrite content is low, and anhydrite is found only at the bottom of the section.

Organic Characteristics

The organic matter types were classified using rock pyrolysis data (HI versus Tmax values, Van Krevelen, 1961; Tissot et al., 1974). The diagram shows that the organic matter in Es4s samples is dominated by type I kerogen and type II kerogen (**Figure 3A**). The vitrinite reflectance values range from 0.65% to 0.77%, and most samples are mature and plot in the oil generation window.

The TOC content of Es4s samples ranges from 0.58% to 1.57% (average 2.4%). S1 ranges from 0.54 mg/g to 9.62 mg/g, with an average of 4.2 mg/g, while S2 ranges from 1.99 mg/g to 31.52 mg/g, with an average of 16 mg/g. The HI values range from 350–700 mg HC/g TOC, with an average of 584 mg HC/g TOC, and the Tmax values range from 418 to 447°C, with an average of 442°C. Proportional to water depth and reducing conditions (Andrea, 2010; Slatt et al., 2012), the relative hydrocarbon generation potential (RHP; that is, S1 + S2/TOC) ranges from 4.36 to 8.95 mg HC/g TOC (with an average of 7.7 mg HC/g TOC) (**Figures 2**, **3**). The results show that the shale samples are rich in organic matter and high in TOC. S1 is positively correlated with TOC (**Figure 3B**). The cross plot of S1 and TOC shows that most of the samples have indigenous hydrocarbons and a small part has nonindigenous hydrocarbons (Jarvie and Baker, 1984; Li et al., 2017b). The relationship between S2 and TOC is a useful indicator for evaluating the hydrocarbon generation potential of source rocks (Peters, 1986; Peters and Cassa, 1994; Alias et al., 2012; Shalaby et al., 2012; Zhao et al., 2014). According to the ratio diagram of S2 to TOC, the NY1 shale sample has good hydrocarbon generation potential (**Figure 3C**).

Lithofacies Description

Based on previous works on lithofacies classification (Dong et al., 2015; Liang et al., 2018b; Chen et al., 2017; Zhang et al., 2018), the mineral compositions (three end members of clay, carbonates, and quartz and feldspar), TOC contents (<2.0% as organic-poor, 2.0–3.5% as intermediate-organic, and >3.5% as organic-rich) and sedimentary structure characteristics (thin-bedded, laminated, and shaly structures), were considered in this study, with seven different lithofacies types identified in the Es4s shale samples. The detailed characteristics of these lithofacies are shown in **Figure 4** and **Table 2**.

Organic-rich calcareous shale: The hand samples are dark gray, rich in carbonate clay minerals and organic matter, and have a foliation structure (**Figure 4A**). The organic matter content is greater than 3.5%, the carbonate content is generally greater than 75%, and calcite veins are present. The laminae are well developed and clearly bounded, consisting of light and dark laminae. The light laminae are calcite veins, and the dark laminae are organic-rich clay minerals (**Figures 4A,B**), with abundant framboidal pyrite (**Figure 4N**). This lithofacies is generally developed in the middle and lower parts of Es4s.

Organic-rich laminated calcareous mudstone: The hand samples are dark gray but lighter in color than the organic-rich calcareous

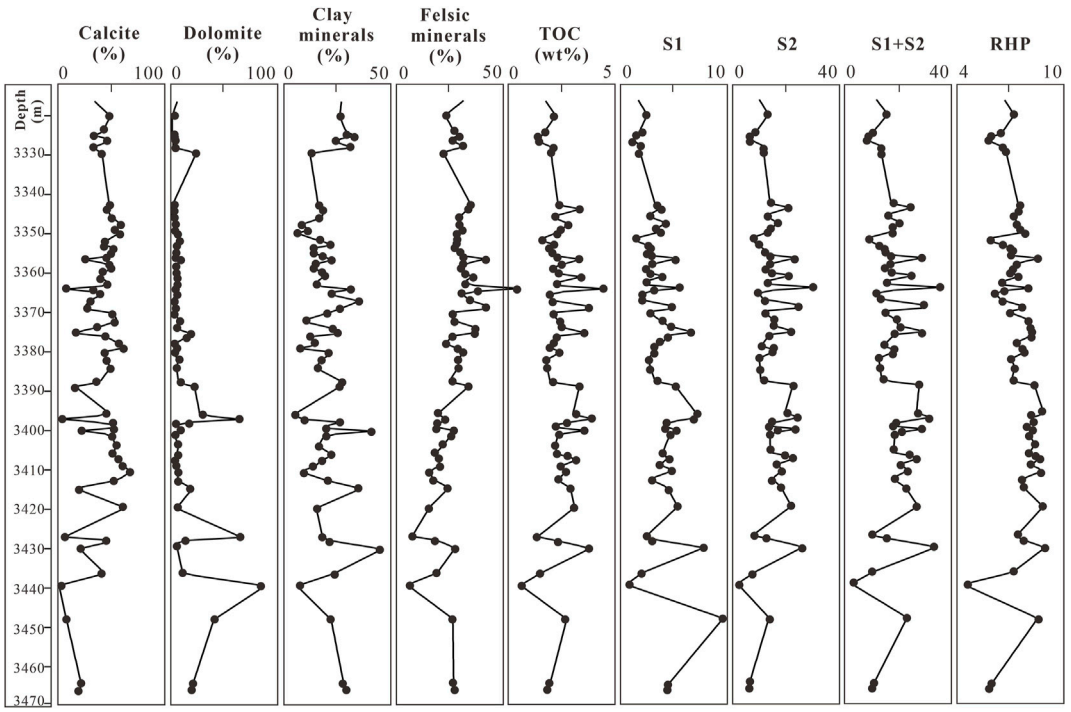

FIGURE 2 | Characteristics of mineral composition and pyrolysis parameters of NY1 samples.

shale and rich in carbonate clay minerals and organic matter (**Figure 4C**). The content of organic matter is greater than 3.5%, and the content of carbonate is greater than 75%, but it is generally lower than that in organic-rich calcareous shale. Granular calcite grains of different sizes are present (**Figure 4D**) with obvious laminae and boundaries, and framboidal pyrite is developed. This lithofacies is mainly developed in the middle and lower parts of the upper Fourth Member of the Shahejie Formation.

Organic-rich laminated carbonate-bearing mudstone: The hand samples are dark gray and rich in clay minerals (**Figure 4E**). The content of organic matter is greater than 3.5%, the content of clay minerals is generally between 60 and 70%, and the carbonate mineral content is low. Granular calcite laminae are mainly developed in the form of interbedded organic matter and clay minerals, and framboidal pyrite is present (**Figure 4F**). This lithofacies is mainly developed in the middle of the upper Fourth Member of the Shahejie Formation.

Intermediate-organic laminated calcareous mudstone: The hand samples are gray in color and are rich in carbonate and clay minerals (**Figure 4G**). The organic matter content varies between 2 and 3.5%, carbonate content is greater than 65%, and micritic calcite laminae are well developed but variable (**Figure 4H**).

Organic-poor laminated calcareous mudstone: The hand samples are gray, but the color is lighter than that of the intermediate-organic laminated calcareous mudstone. These samples are rich in carbonate and clay minerals (**Figure 4I**). The content of organic matter is less than 2%, and the carbonate mineral content is generally greater than 50%. The laminae are slightly developed, but the boundaries are not obvious (**Figure 4J**).

Organic-poor thin-bedded calcareous mudstone: The hand samples are gray, lighter in color than all other lithofacies, and rich in carbonate minerals and clay minerals (**Figure 4K**). The content of organic matter is less than 2%, and the content of carbonate minerals is greater than 50%, but the content of dolomite is significantly higher than that of calcite. The dolomite is distributed in clay minerals in the form of micrite (**Figure 4O**), and laminae are not developed (**Figure 4L**).

Laminated silty mudstone: This lithofacies is rich in felsic minerals and clay minerals and generally has high organic matter contents (3.5% on average). Compared with the other lithofacies, this lithofacies has the highest contents of felsic minerals (up to 45%) and pyrite. This lithofacies is well laminated and characterized by interbedded organic matter and clay minerals (**Figure 4M**). Granular quartz is usually surrounded by clay minerals and mainly exists in the form of terrigenous detrital material. This lithofacies is mainly developed in the middle and upper parts of Es4s.

Major and Trace Element Geochemistry

Suitable environmental indicators can better reflect the evolution of the paleoenvironment. The chemical index of alteration (CIA) is often used as an index to evaluate the intensity of weathering and the climate (Price and velbel, 2003). The CIA data in this paper are from Chao, Liang (2018). Generally, the element enrichment coefficient is used to indicate whether the element content in sediments is enriched or depleted relative to the standard content (Taylor and Mclennan, 1985; Walsh et al., 1988; Murray et al., 1992; Saito, 1992; Algeo and Liu, 2020). In addition, since the TOC content is usually closely related to

TABLE 1 | The mineral composition of the Es4s shale in Well Ny1.

Sample	Clay (%)	Feldspar (%)	Quartz (%)	Calcite (%)	Dolomite (%)	Pyrite (%)	Anhydrite (%)
1	27	4	28	30	7	4	—
2	26	2	20	49	1	2	—
3	29	2	24	42	1	2	—
4	34	3	26	34	1	2	—
5	22	2	22	51	2	1	—
6	33	3	29	31	2	2	—
7	12	1	20	41	24	2	—
8	16	2	31	48	1	2	—
9	18	3	30	46	1	2	—
10	18	2	27	50	1	2	—
11	7	1	27	60	4	1	—
12	13	1	31	52	2	1	—
13	6	1	27	58	7	1	—
14	16	1	26	46	9	2	—
15	24	4	23	41	5	3	—
16	13	1	25	53	6	2	—
17	13	1	29	50	5	2	—
18	18	2	27	49	2	2	—
19	23	3	39	22	11	2	—
20	14	2	29	49	4	2	—
21	13	2	27	51	5	2	—
22	20	2	29	42	5	2	—
23	18	3	31	39	6	3	—
24	13	2	27	52	4	2	—
25	32	3	53	6	3	3	—
26	19	2	27	45	5	2	—
27	35	3	30	29	1	2	—
28	26	3	41	24	3	3	—
29	20	1	24	51	2	2	—
30	8	1	24	56	9	2	—
31	23	4	32	35	3	3	—
32	27	4	31	12	19	7	—
33	12	2	24	45	15	2	—
34	16	2	20	58	2	2	—
35	7	1	26	61	4	1	—
36	23	3	28	42	2	2	—
37	17	2	26	46	7	2	—
38	15	3	25	49	5	3	—
39	28	2	22	39	7	2	—
40	26	2	31	16	22	3	—
41	4	1	18	50	27	0	—
42	9	1	22	2	66	0	—
43	31	4	17	42	3	3	—
44	11	2	14	63	8	2	—
45	43	6	18	20	8	5	—
46	19	3	22	50	3	3	—
47	16	2	19	54	7	2	—
48	23	4	13	52	5	3	—
49	18	3	16	57	4	2	—
50	14	3	17	61	3	2	—
51	7	2	13	69	7	2	—
52	20	3	14	56	6	1	—
53	36	6	17	16	20	5	—
54	15	3	12	63	5	2	—
55	18	2	5	6	66	3	—
56	22	4	14	54	4	2	—
57	46	8	18	20	6	2	—
58	23	5	13	44	11	4	—
59	6	2	3	1	88	0	—
60	22	7	18	8	40	5	—
61	28	8	18	22	20	4	—
62	30	8	18	20	19	4	1

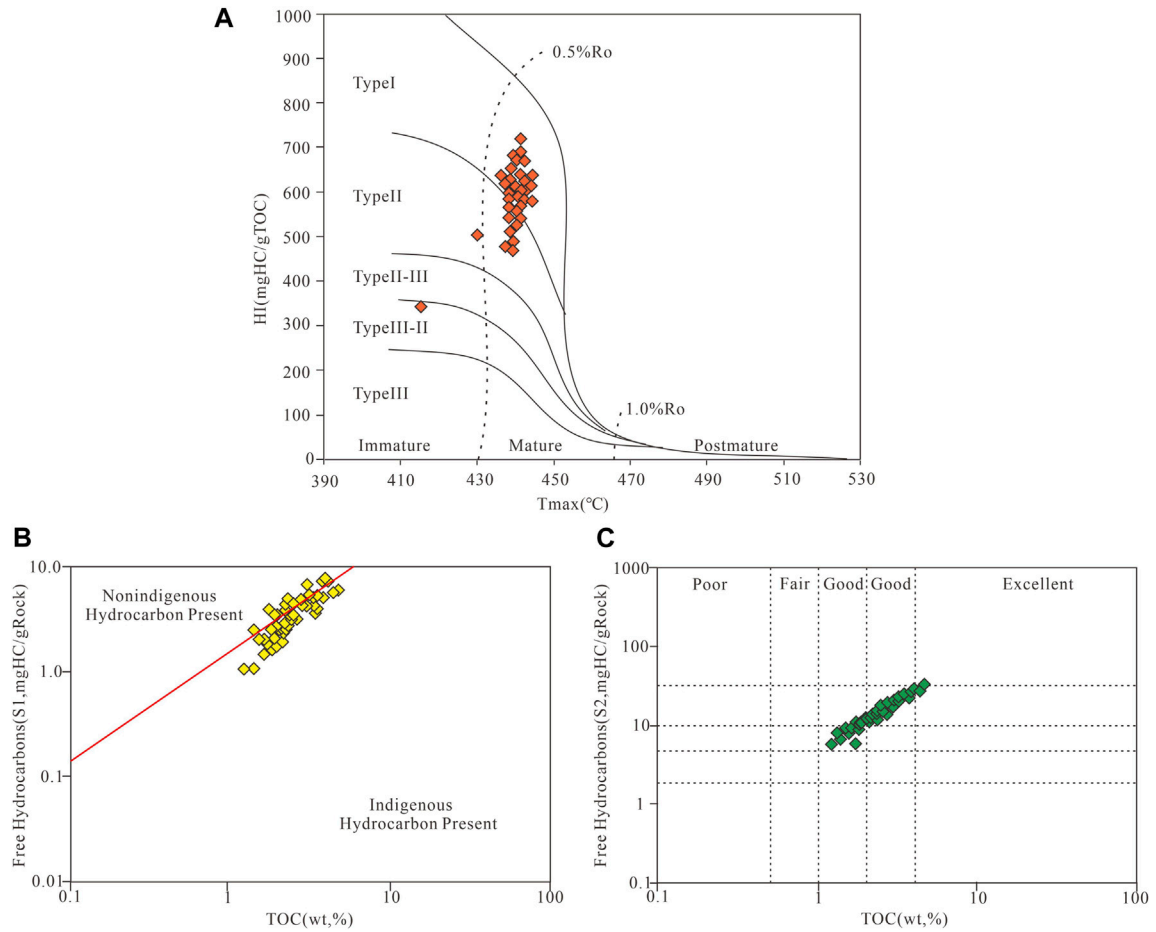

FIGURE 3 | Organic geochemical characteristics of the Es4s shale. **(A)** A plot of the HI of the sample relative to the maximum pyrolysis temperature (Tmax) of the pyrolysis product, reflecting the kerogen mass and thermal maturity stage (boundary modified by Mukhopadhyay et al., 1995). **(B)** Free hydrocarbons (S1) versus total organic carbon (TOC). **(C)** Pyrolytic hydrocarbon (S2) and TOC plots after kerogen cracking, showing source rock potential (boundaries revised by Peters and Cassa, 1994).

redox conditions, TOC can also be used as an indicator to reconstruct the redox conditions (Dong et al., 2018). The strontium abundance and Sr/Ba ratio can be used as sensitive indicators of paleosalinity. Therefore, the Sr abundance and Sr/Ba ratio recorded in sediments are significantly positively correlated with paleosalinity (Zheng and Liu, 1999). Siliceous organisms and authigenic quartz are scarce in the saltwater basin, so the content of felsic minerals can be used as a good indicator to evaluate terrigenous input. The Fe/Mn ratio can be used as a marker of offshore distance (or water depth) (Chen et al., 2008). It has been confirmed that Ba has a positive correlation with surface productivity and organic matter enrichment in water and has been widely used in evaluations of paleoproductivity (Dymond et al., 1992; Li et al.,. 2015; Teng, 2006).

The results show that the Sr/Ba ratio of the tested shale samples varies between 0.25 and 13.23, with an average of 2.88. The Mn/Fe ratio varies between 0.02 and 0.14, with an average of 0.06. In addition, Mn/Fe and Sr/Ba ratios vary greatly. The Sr/Ba ratio of the middle and lower strata of Es4s (mean value: 7.33) is much higher than that of the upper strata of Es4s (mean value: 0.55). The Mn/Fe ratio (mean value: 0.04) is the lowest in the lower strata of Es4s, followed by the Mn/Fe ratio (mean value: 0.055) in the upper strata and the Mn/Fe ratio (mean value: 0.075) in the middle strata (**Figure 5** and **Table 3**). **Figure 5** shows that the Mn/Fe and Sr/Ba ratios in the upper submember of the Fourth Member of the Shahejie Formation are negatively correlated; from bottom to top, the Mn/Fe ratios tend to increase gradually, although the ratios tend to decrease slightly in the upper strata. The Sr/Ba ratio gradually decreases.

DISCUSSION

Evolution of Sedimentary Environments Under a High-Precision Sequence Stratigraphic Framework

The development of mineral characteristics and sequence stratigraphy is controlled by the sedimentary environment. Therefore, it is very important to analyze the evolution of the

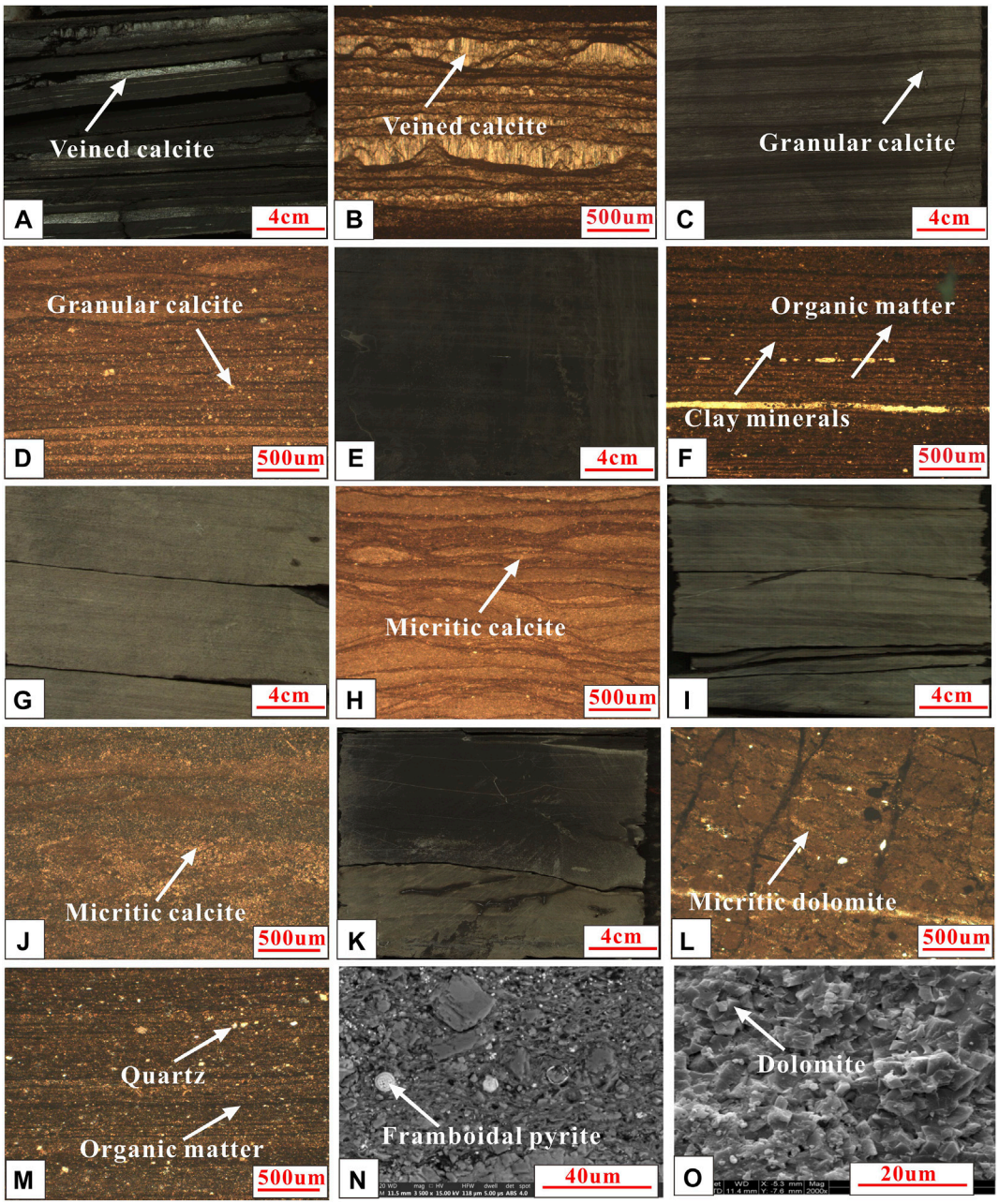

FIGURE 4 | Es4s shale cores and micrographs. **(A,B)** Organic-rich calcareous shale samples showing veined calcite laminae, thicker than clay laminae. Thin section photographs are viewed under orthogonal light (3,438.12 m, Well NY1). **(C,D)** Organic-rich laminated calcareous mudstone with granular calcite as the main material. Thin section photographs are viewed under orthogonal light (3,418.42 m, Well NY1). **(E,F)** Organic-rich laminated carbonate-bearing mudstone mainly interbedded with organic matter and clay minerals. Thin section photographs are viewed under plane-polarized light (3,423.23 m, Well NY1). **(G,H)** Intermediate-organic laminated calcareous mudstone mainly containing micritic calcite laminate. Thin section photographs are viewed under orthogonal light (3,421.47 m, Well NY1). **(I,J)** The organic-poor thin-bedded calcareous mudstone has no distinct boundary. Thin section photographs were taken under orthogonal light (3,325.99 m, Well NY1). **(K,L)** Organic-poor thin-bedded calcareous mudstones with undeveloped laminae and carbonate minerals dominated by micritic dolomite. Thin section photographs are viewed under plane-polarized light (3,465.45 m, Well NY1). **(M)** Laminated silty mudstone with an organic matter and clay mineral interlayer. Thin section photographs are viewed under plane-polarized light (3,382.16 m, Well NY1). **(N)** Framboidal pyrite is abundant in organic-rich calcareous shale (3440.12 m,well NY1). **(O)** Micritic dolomites are found in organic-poor thin-bedded calcareous mudstone (3450.73 m, well NY1).

sedimentary environment through high-precision sequence stratigraphy division. The GRP method proposed and improved by Slatt et al. (2008), Slatt et al., 2012) mainly divides GRP cycles according to the superposition combination pattern of natural GR curves. Abouelresh and slatt, (2012) applied TH and U curves and combined them

TABLE 2 | The main lithofacies development characteristics of Es4s in the Dongying depression.

Basis of division	Lithofacies	Color	Mineral composition	TOC contient	Laminated characteristics
Major or special types and amounts of minerals; TOC; Sedimentary structures	Organic-rich calcareous shale	Dark gray	Carbonate content is generally above 75%., calcite veins are developed, with abundant strawberry pyrite	Above 3.5%	Well developed and clearly bounded, consisting of light and dark laminae. The light laminae are calcite veins, and the dark laminae are organic-rich clay minerals
	Organic-rich laminated calcareous mudstone	Dark gray	Carbonate content is generally above 75%, Granular calcite are developed, with abundant strawberry pyrite	Above 3.5%	Well developed and clearly bounded. consisting of light and dark laminae. The light laminae are Granular calcite, and the dark laminae are organic-rich clay minerals
	Organic-rich laminated carbonate-bearing mudstone	Dark gray	Clay minerals content is generally between 60 and 70%, with abundant strawberry pyrite	Above 3.5%	Well developed and clearly bounded
	Intermediate-organic laminated calcareous mudstone	Gray	Carbonate content is more than 65%	Between 2 and 3.5%	Laminae developed and fluctuated, dominated by micritic calcite
	Organic-poor laminated calcareous mudstone	Light gray	Carbonate content is more than 50%	Less than 2%	Laminae are slightly developed but not obvious
	Organic-poor thin-bedded calcareous mudstone	Light gray	Carbonate content is more than 50%, the content of dolomite is significantly higher than that of calcite	Less than 2%	Lamina is not developed
	Laminated silty mudstone	Dark gray	felsic content (up to 45%), with some strawberry pyrite	(3.5% on average)	Laminae developed

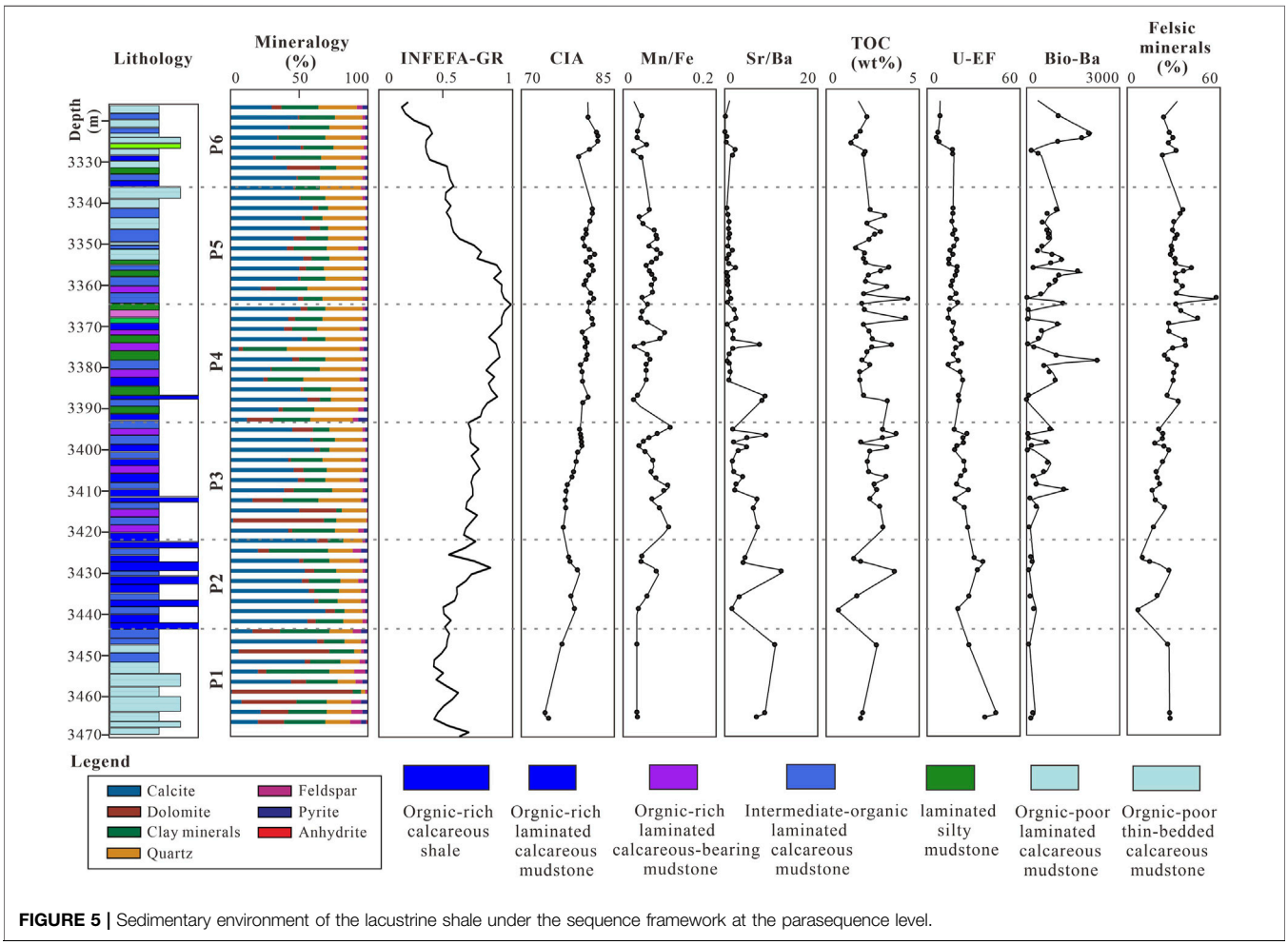

FIGURE 5 | Sedimentary environment of the lacustrine shale under the sequence framework at the parasequence level.

TABLE 3 | Geochemical data of the Es4s shale in Well NY1.

No	Inorganic element parameters							Organic geochemical parameters			
	Fe ug/g	Ba ug/g	U ug/g	Al wt%	Ti ug/g	Sr ug/g	Mn ug/g	TOC wt%	RHP	Tmax	HI
1	2,682.00	127.00	2.00	0.68	205.00	181	42	1.62	6.53	442	562.96
2	5,639.00	1,075.00	4.00	1.39	406.00	284	233	2.23	7.21	443	608.07
3	10,189.00	2,153.00	7.00	2.84	1,050.00	452	349	1.70	6.61	441	553.53
4	9,148.00	1976.00	4.00	2.06	682.00	567	313	1.58	6.36	442	502.53
5	3,220.00	830.00	2.00	0.85	179.00	228	190	1.23	5.54	442	466.67
6	6,131.00	112.00	3.00	0.52	428.00	320	131	2.12	6.58	441	562.26
7	15,308.00	552.00	9.00	1.49	1,590.00	782	551	2.00	6.74	441	583.00
8	11,893.00	1,062.00	6.00	1.03	887.00	601	709	2.34	7.44	442	604.27
9	17,225.00	842.00	9.00	1.58	1,565.00	751	554	3.39	7.46	442	633.92
10	18,051.00	659.00	8.00	1.45	1,533.00	721	651	2.05	7.20	441	596.59
11	9,887.00	799.00	7.00	1.11	840.00	716	711	2.93	7.41	443	586.69
12	9,321.00	805.00	6.00	1.04	938.00	694	573	2.44	7.43	442	612.70
13	11,999.00	811.00	7.00	1.05	814.00	762	939	2.30	7.96	441	630.87
14	11,569.00	578.00	8.00	1.32	1,169.00	569	499	1.40	5.52	441	475.71
15	12,602.00	428.00	6.00	1.19	985.00	745	964	2.18	—	—	—
16	12,047.00	1,056.00	7.00	1.18	890.00	894	938	1.92	6.91	444	539.58
17	8,580.00	1,208.00	5.00	1.08	804.00	575	572	2.06	7.32	444	604.37
18	12,156.00	830.00	6.00	1.32	1,099.00	714	655	2.16	6.78	444	567.59
19	13,699.00	238.00	10.00	1.43	1,292.00	647	683	3.50	8.80	444	718.86
20	15,552.00	1964.00	8.00	1.23	1,146.00	877	994	2.61	7.33	446	606.13
21	15,276.00	978.00	8.00	1.27	1,089.00	865	1,076	2.09	7.23	445	600.00
22	12,803.00	1,069.00	8.00	1.38	1,214.00	782	942	2.15	6.90	444	581.40
23	11,553.00	772.00	7.00	1.33	1,189.00	670	700	3.41	7.54	447	636.66
24	10,492.00	528.00	6.00	0.90	728.00	612	720	1.82	6.13	443	524.18
25	14,357.00	190.00	7.00	1.45	2,252.00	272	506	4.57	8.16	444	689.72
26	15,571.00	1,495.00	10.00	1.33	1,154.00	695	959	1.88	6.03	442	494.15
27	561.00	13.00	1.00	0.21	51.00	29	21	2.08	6.47	444	555.29
28	8,076.00	129.00	5.00	1.00	917.00	377	297	4.40	7.95	443	667.27
29	12,302.00	1,194.00	8.00	1.26	1,071.00	697	691	1.98	6.82	442	548.99
30	12,563.00	499.00	4.00	0.73	380.00	920	1,149	2.36	8.04	442	650.42
31	9,433.00	454.00	7.00	1.11	801.00	821	771	2.48	8.17	440	628.23
32	34,552.00	79.00	10.00	1.29	1,370.00	692	422	3.77	8.21	439	636.07
33	10,810.00	417.00	7.00	1.14	677.00	733	641	2.26	8.22	445	623.45
34	13,651.00	1,145.00	9.00	1.55	1,240.00	958	601	2.15	7.26	444	543.26
35	15,346.00	2,381.00	9.00	1.29	900.00	1,442	1,029	1.91	7.52	446	578.01
36	7,187.00	616.00	5.00	1.27	855.00	825	355	2.50	7.94	445	668.80
37	19,774.00	900.00	12.00	1.62	1,302.00	1,407	1,014	1.80	7.04	443	556.11
38	12,907.00	1,030.00	11.00	1.36	1,174.00	939	650	1.82	7.24	444	570.33
39	13,951.00	89.00	9.00	1.26	1,000.00	804	361	1.97	7.06	441	541.12
40	24,114.00	115.00	13.00	1.82	1973.00	936	569	3.34	8.34	443	681.74
41	10,186.00	846.00	8.00	1.33	493.00	1,373	1,188	3.02	8.88	443	651.66
42	28,859.00	97.00	13.00	1.44	1780.00	971	1,138	3.98	8.17	443	638.19
43	16,950.00	248.00	14.00	1.78	1962.00	1,025	519	2.80	8.35	445	—
44	8,869.00	722.00	9.00	1.10	515.00	1,408	1,227	1.80	7.94	441	—
45	21,465.00	110.00	12.00	2.03	1922.00	664	254	3.70	8.20	446	—
46	8,709.00	293.00	8.00	1.27	971.00	801	440	2.35	8.00	443	—
47	13,515.00	799.00	11.00	1.30	758.00	1,322	996	2.20	8.38	442	—
48	12,389.00	653.00	11.00	1.31	1,081.00	1,218	803	2.29	8.01	447	—
49	11,623.00	304.00	9.00	1.26	1,102.00	1,238	674	3.33	8.70	446	—
50	8,772.00	407.00	8.00	1.23	791.00	1,107	849	2.41	8.06	445	—
51	20,846.00	1,384.00	11.00	1.18	924.00	2,644	2085	2.76	8.94	443	—
52	10,136.00	171.00	9.00	1.56	1,011.00	1,282	632	2.30	7.64	446	—
53	8,320.00	351.00	8.00	0.94	393.00	2,176	629	2.91	7.71	440	—
54	6,966.00	123.00	7.00	0.77	829.00	891	707	3.11	8.83	447	—
55	24,469.00	202.00	7.00	0.66	656.00	891	710	1.37	7.34	440	—
56	13,677.00	293.00	12.00	0.94	1,334.00	1,103	668	2.22	7.64	446	—
57	6,052.00	69.00	7.00	0.64	602.00	913	455	3.85	8.95	442	—
58	6,387.00	236.00	8.00	0.86	1,168.00	710	294	1.51	7.11	445	—
59	1976.00	244.00	2.00	0.30	107.00	378	67	0.58	4.36	443	—
60	2,820.00	37.00	3.00	0.32	250.00	409	91	2.74	8.53	433	501.82
61	11,020.00	294.00	11.00	0.70	926.00	2,583	385	1.95	—	—	—
62	7,627.00	125.00	8.00	0.75	817.00	682	251	1.74	5.74	418	336.21

with GRP theory to divide the sequences of the Barnett shale in the United States and proposed that the RHP could also be used as an index for sequence division. The INPEFA method proposed by a research team in the Netherlands mainly uses GR curves to analyze spectrum attributes and obtain an INPEFA curve (Nio et al., 2005), thus realizing the division of sequence stratigraphy (Liu et al., 2019; Ma et al., 2016; Ma et al., 2021). Based on the INPEFA of the GR curve and combined with the analysis of environmental indicators, we divided the upper submember of the Fourth Member of the Shahejie Formation from bottom to top into six parasequences (**Figure 5**).

In P1 (3,444.17–3,470.15 m depth range), the GR curve has a low INPEFA curve, and the CIA index is low, ranging from 73.715–76.346 (average 75.035), indicating that the climate was cold and dry, and the water body was shallow, corresponding to a low Mn/Fe ratio. The Sr/Ba ratio is high, with an average value of 8.43, indicating a high salinity, which may be related to the abundant gypsum at the bottom. The low TOC value in this section is 1.75% on average, and the RHP value is 2.87 mg HC/g TOC, indicating that the reducing conditions in this section were weak, which is not conducive to the preservation of organic matter. In addition, this result is consistent with the low enrichment coefficient of U and the lowest Bio-Ba value, indicating that the primary productivity was very low. In this period, the climate was relatively dry and cold, with little precipitation and shallow water, leading to weak reducing conditions, high salinity, a lack of biological development, low primary productivity and a low organic matter content.

In P2 (depth range 3,423.80–3,444.17 m), the INPEFA curve of the GR curve shifted significantly to the right, the CIA index increased significantly, and the increase in the Mn/Fe ratio indicates that the climate became warm and humid during this period. The water body became significantly deeper, and the Sr/Ba ratio decreased greatly, with an average value of 5.19, indicating that the salinity decreased. The development of framboidal pyrite in this period and the high TOC (average 2.5%) and high RHP (average 7.76 mg HC/g TOC) in this section indicate that the water conditions in this period were highly reducing, conducive to the preservation of organic matter, and that the Bio-Ba values were low, indicating low primary productivity. In this period, the climate was wet and warm, and the precipitation increased, leading to the deepening of the lake and a low salinity.

In P3 (depth range 3,393.34–3,423.80 m), the INPEFA curve of the GR curve continued to shift to the right, and the CIA index and Mn/Fe ratio continued to increase, indicating that the climate continued to become warmer and more humid and that the water depth further increased. The Sr/Ba ratio decreased to an average of 4.26, and the salinity continued to decrease. The average TOC was 2.7%, and the average RHP was 8.27 mg HC/g TOC, indicating that the water conditions in this period were highly reducing and conducive to the preservation of organic matter. In addition, the Bio-Ba value increased, indicating that the primary productivity increased in this period.

In P4 (depth range 3,362.70–3,393.34 m), the INPEFA curve of the GR curve has the largest rightward deviation, and the CIA index is the highest, with an average of 80.603, indicating that the water body reached its deepest depth at this time. The Sr/Ba ratio further decreases, with an average value of 2, indicating that the salinity of water at this time was significantly lower than that in P3. The enrichment coefficient of U is lower than that in P3. The mean TOC is 2.53%, and the RHP is 7.45 mg HC/g TOC, indicating strong reducing conditions in this period but weaker than those in P3. The maximum value of Bio-Ba and the maximum value of felsic minerals indicate the maximum primary productivity and terrigenous detrital input during this period. During this period, the climate was very wet and warm, and the precipitation was abundant, which allowed the water depth to reach the maximum; the salinity was further reduced, terrigenous debris was abundant, the primary productivity was high, and the water conditions were strongly reducing, which led to enrichment of organic matter in the sediment.

In P5 and P6 (depth range 3,336.81–3,336.81 m), the INPEFA curve of the GR curve began to deviate to the left, the CIA index decreased slightly, with an average of 80.60, and Mn/Fe decreased slightly, indicating that the water depth decreased at this time. The Sr/Ba ratio decreased with an average value of 0.97, indicating that the salinity of water further reduced the TOC by 2.00% and RHP by 6.17 mg HC/g TOC, indicating that the reducing conditions of the water weakened further in this period, but the reduction was stronger than in P1. During this period, the Bio-Ba value decreased, and the felsic mineral content decreased overall, indicating that primary productivity decreased and terrigenous detrital input decreased. During this period, the climate became slightly drier and cooler, and the water body decreased in size. However, the input of terrigenous debris and the existence of primary productivity during this period reduced the salinity of the water body, weakened the reducing conditions of the water body, and led to a decrease in organic matter abundance.

In general, the climate during the deposition of Es4s shifted from relatively dry to wet to a slightly drier and cooler. The salinity gradually decreased, the TOC and U element enrichment coefficients first decreased and then increased, and the reducing conditions of the water first decreased and then increased.

Corresponding Characteristics of Lithofacies Assemblages in Different Sedimentary Environments

The regular change in sedimentary environment controls the regular change in mineral composition and sedimentary structure, which leads to the regular change in the vertical lithofacies assemblage (Liang et al., 2018a; Zeng et al., 2021; Wu et al., 2020; Zhang et al., 2022b). The climate of the P1 parasequence was dry and cold, with little precipitation, resulting in shallow water, easy destruction of laminar structure and weak reducing conditions, which were not conducive to the preservation of organic matter. In addition, gypsum minerals developed at the bottom, indicating a higher salinity and more carbonate minerals in the area, with an average of approximately 40%. However, the content of dolomite is generally higher than the calcite content, which is caused by a dry and cold climate. In summary, the influence of the above factors led to the

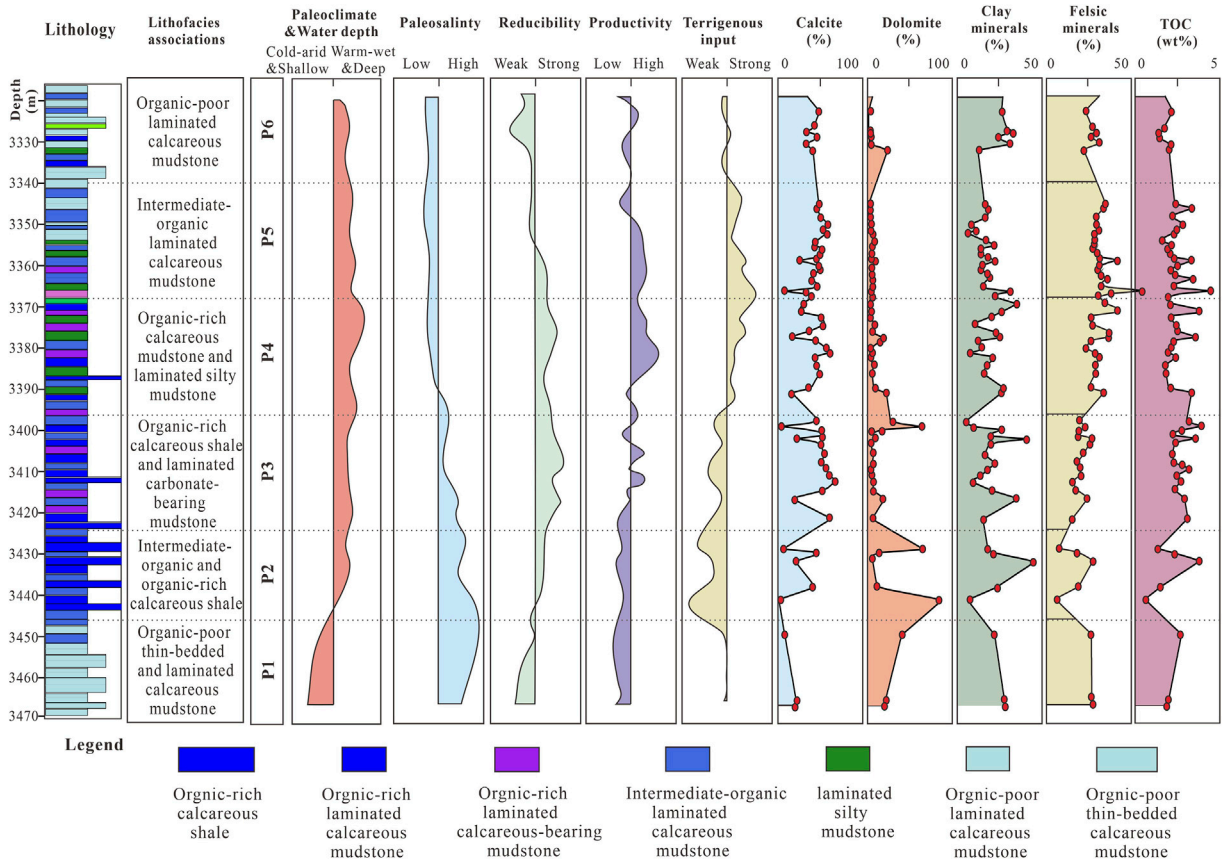

FIGURE 6 | Evolution model of the sedimentary environment of the upper Es4s shale.

development of a lithofacies combination involving organic-poor thin-bedded calcareous mudstone and organic-poor laminated calcareous mudstone. During the P2 parasequence period, the climate became very wet and warm, and the rainfall increased. As a result, the water deepened rapidly, the salinity decreased, the reducing conditions increased, the organic matter was well preserved, and the laminar structure was well developed. In addition, carbonate minerals were dominant in this period, and the calcite content was higher than the dolomite content, so the lithofacies assemblage of organic-rich calcareous shale and organic-rich laminated calcareous mudstone was predominant in this period. As the climate became wetter and warmer, the water became deeper, leading to a further decrease in salinity, stronger reducing conditions, increased input of terrigenous detritus, and increased primary productivity. The organic matter was preserved and abundant in the P3 parasequence. The lithofacies assemblage is mainly composed of organic-rich laminated carbonate-bearing mudstone and organic-rich laminated calcareous mudstone. In the P4 period, the climate became humid and warm, and the precipitation increased further, which further deepened the water body, reduced the salinity, and strengthened the reducing conditions. Terrigenous detritus, primary productivity and organic matter were abundant in this period. However, terrigenous detritus also disrupted the reducing conditions to a certain extent. The lithofacies in this stage were mainly composed of laminated silty mudstone and organic-rich laminated calcareous mudstone. During the parasequence periods of P5 and P6, the climate became slightly drier and cooler, and the water depth and reducing conditions decreased. Moreover, terrigenous clastics were more abundant during this period, diluting the water salinity to a certain depth. The lithofacies were mainly laminated calcareous mudstones with intermediate and low amounts of organic matter (**Figure 6**).

Effects of Paleoclimate on Lake Water Properties at the Parasequence Level

The paleoclimate plays a decisive role in the enrichment and preservation of organic matter by controlling the depth of the water body, influencing the supply of terrestrial matter, and controlling the primary productivity of the water body, all of which influence the redox conditions (Liang et al., 2018b; Zhang et al., 2022c). The data show that the CIA is positively correlated with the Mn/Fe ratio and negatively correlated with the Sr/Ba ratio (**Figures 7A,B**), indicating that the paleoclimate had a significant influence on the paleosalinity by controlling the paleowater depth. A dry and cold climate leads to stronger

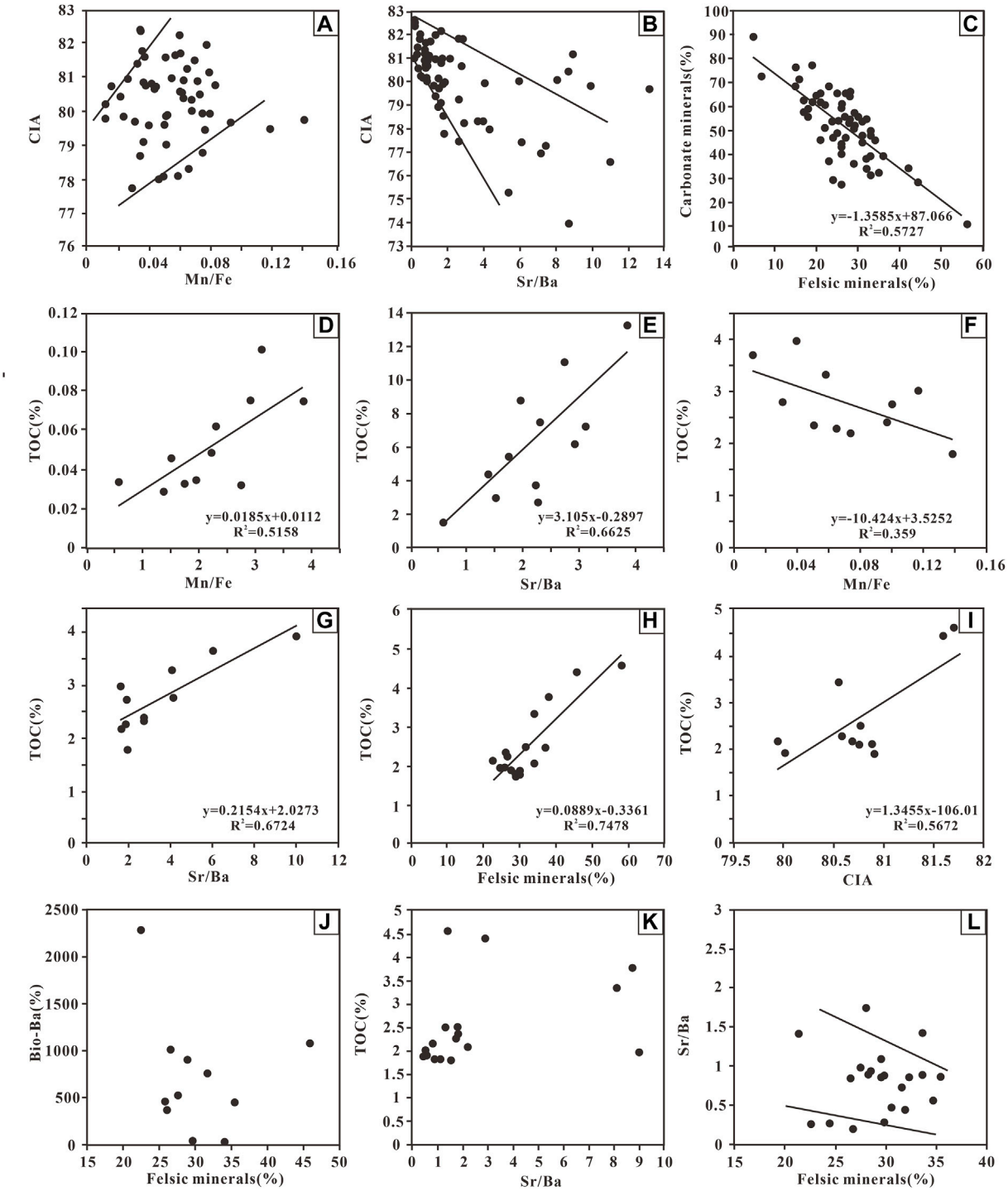

FIGURE 7 | Relationships between different geochemical parameters of the Es4s shale.

evaporation and less precipitation, which increases the salinity of lake water. As the climate becomes wetter and warmer, evaporation weakened, and precipitation increases, leading to a decrease in salinity. In addition, a high salinity increases the ion concentration of the water, which promotes carbonate precipitation, and a humid climate leads to a greater supply of terrigenous material. The data show that felsic minerals are positively correlated with carbonate minerals (**Figure 7C**), which indicates that terrigenous input can dilute the salinity of water and indirectly proves that a humid climate can reduce the

salinity of water. The data also show that the Mn/Fe ratio is positively correlated with TOC during the P1 and P2 periods (**Figure 7D**), and the Sr/Ba ratio is positively correlated with TOC (**Figure 7E**), indicating that salinity controlled the stratification of the water and enhanced the reducing conditions of the water, which was conducive to the preservation of organic matter. Moreover, the P2 parasequence mainly developed unique vein calcite lithofacies, indicating that the content of carbonate deposited at that time was higher than that of the other parasequences, and the reducing conditions were also stronger. In the P3 parasequence period, the Mn/Fe ratio is negatively correlated with TOC (**Figure 7F**), but the Sr/Ba ratio is positively correlated with TOC (**Figure 7G**), indicating that during this period, due to the humid and warm climate, the lake water deepened, and the salinity further decreased, resulting in a low salinity and slightly weak reducing conditions; however, water stratification still existed, the salinity was still high, and the reducing conditions remained strong. As the climate gradually became wetter and warmer, precipitation continued to increase, and the salinity further decreased. In the P4 parasequence period, the TOC is still high, but the Sr/Ba ratio has a very weak positive correlation with TOC (**Figure 7K**), while the CIA value has an obvious positive correlation with TOC (**Figure 7I**), indicating that the salinity concentration of water at this time was low, and it may not have been sufficient to stratify the lake water. At this time, the lake was mainly stratified by temperature. There is also a significant positive correlation between felsic minerals and TOC (**Figure 7H**), indicating that the wet and warm climate led to abundant terrigenous input, which had a significant dilution effect on water salinity and disrupted the salinity-driven stratification. However, there was no correlation between the Bio-Ba value and the felsic mineral content at this time (**Figure 7J**), indicating that the strong primary productivity at this time was due to algae blooms rather than terrigenous input. Moreover, the crossplot in **Figure 4** also proves this point. During the P5 and P6 periods, the climate became slightly drier and cooler, the depth of the water decreased slightly, and the stratification of water gradually weakened, which was not conducive to the enrichment of organic matter. The ratio of Sr/Ba also gradually decreased, and there was a negative correlation between felsic minerals and the Sr/Ba ratio (**Figure 7L**), indicating that although terrigenous input was not large at this time, it had a dilution effect on water salinity, leading to a decrease in water salinity. In summary, the paleoclimate influenced the salinity and redox environment of the water by controlling the water depth and input of terrigenous debris and finally caused corresponding regular changes in the water properties.

Effects on Organic Matter Enrichment

The factors affecting the enrichment of organic matter in lake water mainly include the redox conditions, primary productivity and input of terrigenous debris (Liang et al., 2017b; Zhang et al., 2022d; Zhang et al., 2020b). During the evolution process of sedimentary environments, these factors jointly affect the enrichment and preservation of organic matter, but they often play different roles, with one or more factors playing a major role. When the climate is dry and cold, the water is shallow and less reducing, which is not conducive to the preservation of organic matter. When the climate is warm and humid, the water is deep, and if the salinity is higher, then salinity-driven stratification will provide stronger reducing conditions. If terrigenous detritus is abundant and the water salinity is low, then temperature-driven stratification will provide strong reducing conditions. In addition, if algal blooms are common, the high primary productivity will also be conducive to the enrichment of organic matter. Therefore, the level of organic matter content is the result of many interrelated factors rather than being affected by a single factor. Therefore, for different periods, a detailed discussion of the changes and relationships of various factors is the main process of analyzing the causes of organic matter enrichment in a given period.

During deposition of the P1 parasequence, the TOC was low, with an average value of 1.75%, and the RHP was 2.87 mg HC/g TOC. At this time, the climate was dry and cold, and the water was shallow, leading to weak reducing conditions and high water salinity, which were not suitable for the survival of plankton. Moreover, the living space of plankton was limited, resulting in a low initial productivity. These results indicate that the enrichment of organic matter in this period was mainly controlled by the redox conditions. The TOC was high (mean 2.5%), and the RHP was also high (mean 7.76 mg HC/g TOC) in the P2 parasequence period. During this period, the climate became very wet and warm, the depth of lake water increased greatly, and the salinity was high, forming salinity-driven stratification, which strengthened the reduction of organic matter and was conducive to the preservation of organic matter. The enrichment of organic matter in this period was mainly controlled by the strong reducing conditions resulting from the water stratification caused by salinity.

In the P3 parasequence, the TOC and RHP averaged 2.7% and 8.27 mg HC/g TOC, respectively, indicating the enrichment of organic matter. At this time, the climate became more humid and warmer, the depth of the lake further increased, and the salinity was further reduced. The water body still retained strong reducing conditions. In addition, planktonic algae were more common in this period, and the primary productivity was higher, which provided a source of organic matter to a certain extent. These phenomena indicate that the organic matter enrichment in this period was mainly controlled by the strong reducing conditions caused by salinity-driven stratification, followed by primary productivity.

In the P4 parasequence period, the degree of humidity and warmth reached the maximum, the water depth also reached the maximum, the average TOC was 2.53%, the average RHP was 7.45 mg HC/g TOC, and the organic matter was relatively abundant. At this time, terrigenous detrital input was abundant, which diluted the water salinity to a certain extent and greatly reduced the water salinity concentration, and the salinity-driven stratification almost disappeared. Due to the very warm and humid climate, high water temperature and great depth of water, temperature-driven stratification occurred in this period, resulting in strong reducing properties. In addition, planktonic algae blooms occurred in this period, and the

primary productivity was very high, so the organic matter was relatively abundant. Organic matter enrichment in this period was mainly controlled by the strong reducing conditions and primary productivity due to stratification caused by temperature, followed by terrigenous detrital input. Moreover, the TOC and RHP values in this period were lower than those of P2 and P3, indicating that salinity-driven stratification was better than temperature-driven stratification in the enrichment and preservation of organic matter, which may be related to the fact that an appropriate saline environment can effectively promote organic matter flocculation and thus improve the capture efficiency of organic matter (Hu et al., 2021).

In the P5 and P6 parasequence periods, the average TOC and RHP values were approximately 1.8% and 6.60 mg HC/g, respectively, which were both low. At this time, the climate became dry and cold, the depth of water decreased, the reducing conditions of the water were weakened, and the living space of plankton was restricted. During this period, some terrigenous debris was imported, which further diluted the salinity of the water and further reduced its salinity.

CONCLUSION

The upper fourth member of the Eocene Shahejie Formation is a typical lacustrine shale in the Bohai Bay Basin. It is mainly composed of carbonate and clay minerals, and the mineral composition is quite different from that of marine siliceous shale. Seven lithofacies types were classified based on core thin section and scanning electron microscope observations, combined with X-ray diffraction and geochemical analysis data. The organic matter in the shale in this area is mainly type I kerogen, with TOC values ranging from 0.58% to 4.57%, with an average of 2.41%, and RHP values ranging from 4.36 mg HC/g TOC to 8.95 mg HC/g TOC, with an average of 7.21 mg HC/g TOC. We introduced the INPEFA curve of the GR curve to divide the studied strata into parasequences, and a total of six parasequences were identified. According to the paleoenvironment indices and lithofacies characteristics, we establish an evolution model diagram of the lacustrine mud shale sedimentary environment and lithofacies assemblage. The results show that the regular change in sedimentary environment controlled the regular change in mineral composition and sedimentary structure, which led to the regular change in vertical lithofacies assemblage. The paleoclimate played a decisive role in the enrichment and preservation of organic matter by controlling the water body depth and subsequently influenced the supply of terrestrial matter, the primary productivity of the water body, and the redox conditions. The enrichment of organic matter was influenced by many interrelated factors rather than a single factor.

DATA AVAILABILITY STATEMENT

The datasets presented in this study can be found in online repositories. The names of the repository/repositories and accession number(s) can be found in the article/ Supplementary Material.

AUTHOR CONTRIBUTIONS

All authors listed have made a substantial, direct, and intellectual contribution to the work and approved it for publication.

FUNDING

This paper is supported by the National Natural Science Foundation of China (NSFC) (Grant No. 41972142; 42102153), China Postdoctoral Science Foundation (Grant No. 2021M693500), Specialized Fund for Shandong Postdoctoral Innovation Project (Grant No. 202103012), and the Fundamental Research Funds for the Central Universities (Grant No. 20CX06086A).

ACKNOWLEDGMENTS

We would like to thank the Exploration and Development Research Institute of Shengli Oil field, SINOPEC, for the provision of original data and publish permission. Thanks to Qianqian Guan and Paulo Joaquim Nota for their contributions to basic data statistics. Special thanks are extended to the editor and reviewers for their constructive comments and suggestions.

REFERENCES

Abouelresh, M. O., and Slatt, R. M. (2012). Lithofacies and Sequence Stratigraphy of the Barnett Shale in East-central Fort Worth Basin, Texas. *Bulletin* 96 (1), 1–22. doi:10.1306/04261110116

Algeo, T. J., and Liu, J. (2020). A Re-assessment of Elemental Proxies for Paleoredox Analysis. *Chem. Geology.* 540, 119549. doi:10.1016/j.chemgeo.2020.119549

Alias, F. L., Abdullah, W. H., Hakimi, M. H., Azhar, M. H., and Kugler, R. L. (2012). Organic Geochemical Characteristics and Depositional Environment of the Tertiary Tanjong Formation Coals in the Pinangah Area, Onshore Sabah, Malaysia. *Int. J. Coal Geology.* 104, 9–21. doi:10.1016/j.coal.2012.09.005

Aplin, A. C., and Macquaker, J. H. S. (2011). Mudstone Diversity: Origin and Implications for Source, Seal, and Reservoir Properties in Petroleum Systems. *Bulletin* 95 (12), 2031–2059. doi:10.1306/03281110162

Boulila, S., Galbrun, B., Huret, E., Hinnov, L. A., Rouget, I., Gardin, S., et al. (2014). Astronomical Calibration of the Toarcian Stage: Implications for Sequence Stratigraphy and Duration of the Early Toarcian OAE. *Earth Planet. Sci. Lett.* 386, 98–111. doi:10.1016/j.epsl.2013.10.047

Chen, Z., Zha, M., and Jin, Q. (2008). Mineral Elemental Response to the Evolution of Terrestrial Faulted-lake basin. *Acta Sedementilogica Sinica* 26, 36–43.

Dong, C., Ma, C., Lin, C., Sun, X., and Yuan, M. (2015). A Method of Classification of Shale Set. *J. China Univ. Pet.* 39 (3), 1–7.

Dong, T., Harris, N., and Ayranci, K. (2018). Relative Sea-Level Cycles and Organic Matter Accumulation in Shales of the Middle and Upper Devonian Horn River Group, Northeastern British Columbia, Canada: Insights into Sediment Flux, Redox Conditions, and Bioproductivity. *GSA Bull.* 130 (5-6), 859–880. doi:10.1130/b31851.1

Dymond, J., Suess, E., and Lyle, M. (1992). Barium in Deep-Sea Sediment: A Geochemical Proxy for Paleoproductivity. *Paleoceanography* 7 (2), 163–181. doi:10.1029/92pa00181

Gao, F. (2021). Influence of Hydraulic Fracturing of strong Roof on Mining-Induced Stress-Insight from Numerical Simulation. *J. Min Strat Control. Eng.* 3 (2), 023032.

Hao, F., Zou, H., and Lu, Y. (2013). Mechanisms of Shale Gas Storage: Implications for Shale Gas Exploration in China. *Bulletin* 97 (8), 1325–1346. doi:10.1306/02141312091

Hill, R. J., Jarvie, D. M., Zumberge, J., Henry, M., and Pollastro, R. M. (2007). Oil and Gas Geochemistry and Petroleum Systems of the Fort Worth Basin. *Bulletin* 91 (4), 445–473. doi:10.1306/11030606014

Hu, T., Pang, X., Jiang, F., Wang, Q., Wu, G., Liu, X., and Chen, Y. (2021). Key Factors Controlling Shale Oil Enrichment in saline Lacustrine Rift basin: Implications from Two Shale Oil wells in Dongpu Depression, Bohai Bay Basin. *Pet. Sci.* 18 (3), 687–711. doi:10.1007/s12182-021-00564-z

Huang, H., Li, R., Jiang, Z., Li, J., and Chen, L. (2020). Investigation of Variation in Shale Gas Adsorption Capacity with Burial Depth: Insights from the Adsorption Potential Theory. *J. Nat. gas Sci. Eng.* 73, 103043. doi:10.1016/j.jngse.2019.103043

Jarvie, D., and Baker, D. (1984). *April). Application of the Rock-Eval III Oil Show Analyzer to the Study of Gaseous Hydrocarbons in an Oklahoma Gas Well* in 187th ACS National Meeting (St. Louis Missouri, 8–13.

Jarvie, D. M., Hill, R. J., Ruble, T. E., and Pollastro, R. M. (2007). Unconventional Shale-Gas Systems: The Mississippian Barnett Shale of north-central Texas as One Model for Thermogenic Shale-Gas Assessment. *Bulletin* 91 (4), 475–499. doi:10.1306/12190606068

Kang, H., Xu, G., Wang, B., Wu, Y., Jiang, P., Pan, J., et al. (2019). Forty Years Development and Prospects of Underground Coal Mining and Strata Control Technologies in China. *J. Mining Strata Control. Eng.* 1 (1), 013501.

Li, Q., You, X., Jiang, Z., Zhao, X., and Zhang, R. (2017). A Type of Continuous Petroleum Accumulation System in the Shulu Sag, Bohai Bay basin, Eastern China. *Bulletin* 101 (11), 1791–1811. doi:10.1306/01251715073

Li, Y., Shao, D., Lv, H., Zhang, Y., Zhang, X., and Zhang, T. (2015). A Relationship between Elemental Geochemical Characteristics and Organic Matter Enrichment in marine Shale of Wufeng Formation-Longmaxi Formation, Sichuan Basin. *Acta Petrolei Sinica* 36 (12), 1470–1483.

Liang, C., Jiang, Z., Cao, Y., Wu, J., Wang, Y., and Hao, F. (2018a). Sedimentary Characteristics and Origin of Lacustrine Organic-Rich Shales in the Salinized Eocene Dongying Depression. *GSA Bull.* 130 (1-2), 154–174. doi:10.1130/b31584.1

Liang, C., Wu, J., Jiang, Z., Cao, Y., and Song, G. (2018b). Sedimentary Environmental Controls on Petrology and Organic Matter Accumulation in the Upper Fourth Member of the Shahejie Formation (Paleogene, Dongying Depression, Bohai Bay Basin, China). *Int. J. Coal Geology.* 186, 1–13. doi:10.1016/j.coal.2017.11.016

Liu, C., Liu, K., Wang, X., Wu, L., and Fan, Y. (2019). Chemostratigraphy and Sedimentary Facies Analysis of the Permian Lucaogou Formation in the Jimusaer Sag, Junggar Basin, NW China: Implications for Tight Oil Exploration. *J. Asian Earth Sci.* 178, 96–111. doi:10.1016/j.jseaes.2018.04.013

Loucks, R. G., and Ruppel, S. C. (2007). Mississippian Barnett Shale: Lithofacies and Depositional Setting of a Deep-Water Shale-Gas Succession in the Fort Worth Basin, Texas. *Bulletin* 91 (4), 579–601. doi:10.1306/11020606059

Ma, Y., Fan, M., Lu, Y., Liu, H., Hao, Y., Xie, Z., Liu, Z., Peng, L., Du, X., and Hu, H. (2016). Climate-driven Paleolimnological Change Controls Lacustrine Mudstone Depositional Process and Organic Matter Accumulation: Constraints from Lithofacies and Geochemical Studies in the Zhanhua Depression, Eastern China. *Int. J. Coal Geology.* 167, 103–118. doi:10.1016/j.coal.2016.09.014

Ma, P., Lin, C., Ren, L., Jahren, J., Dong, D., Yu, G., et al. (2021). Linkage and Growth of the Independent and Coherent Faults: Insight Into the Effect of Relay Ramps on Sedimentation Patterns in the Northern Bonan Sag, Bohai Bay Basin. *Mar. Pet. Geol.* 127, 104985.

Mukhopadhyay, P. K., Wade, J. A., and Kruge, M. A. (1995). Organic Facies and Maturation of Jurassic/Cretaceous Rocks, and Possible Oil-Source Rock Correlation Based on Pyrolysis of Asphaltenes, Scotian Basin, Canada. *Org. Geochem.* 22 (1), 85–104. doi:10.1016/0146-6380(95)90010-1

Murray, R. W., Buchholtz ten Brink, M. R., Gerlach, D. C., Russ, G. P., III, and Jones, D. L. (1992). Interoceanic Variation in the Rare Earth, Major, and Trace Element Depositional Chemistry of Chert: Perspectives Gained from the DSDP and ODP Record. *Geochimica et Cosmochimica Acta* 56 (5), 1897–1913. doi:10.1016/0016-7037(92)90319-e

Nio, S., Brouwer, J., Smith, D., de Jong, M., and Böhm, A. (2005). Spectral Trend Attribute Analysis: Applications in the Stratigraphic Analysis of Wireline Logs. *First Break* 23 (4). doi:10.3997/1365-2397.23.4.26503

Peters, K. E., and Cassa, M. R. (1994). *Applied Source Rock Geochemistry: Chapter 5: Part II*. Essential Elements.

Peters, K. (1986). Guidelines for Evaluating Petroleum Source Rock Using Programmed Pyrolysis. *AAPG Bull.* 70 (3), 318–329. doi:10.1306/94885688-1704-11d7-8645000102c1865d

Price, J., and Velbel, M. (2003). Chemical Weathering Indices Applied to Weathering Profiles Developed on Heterogeneous Felsic Metamorphic Parent Rocks. *Chem. Geology.* 202 (3-4), 397–416. doi:10.1016/j.chemgeo.2002.11.001

Rodriguez, N. D., and Philp, R. P. (2010). Geochemical Characterization of Gases from the Mississippian Barnett Shale, Fort Worth basin, Texas. *Bulletin* 94 (11), 1641–1656. doi:10.1306/04061009119

Rowe, H., Hughes, N., and Robinson, K. (2012). The Quantification and Application of Handheld Energy-Dispersive X-ray Fluorescence (ED-XRF) in Mudrock Chemostratigraphy and Geochemistry. *Chem. Geology.* 324-325, 122–131. doi:10.1016/j.chemgeo.2011.12.023

Saito, C. (1992). Particulate Flux of Al. A Compoent of Land Origin, in the Western North Pacific. *Deep-sea Res.* 39, 169–184. doi:10.1016/0198-0149(92)90071-z

Slatt, R., Philp, P., Abousleiman, Y., Singh, P., Perez, R., Portas, R., et al. (2012). *Pore-to-regional-scale Integrated Characterization Workflow for Unconventional Gas Shales*.

Taylor, S., and McLennan, S. (1985). *The continental Crust: Its Composition and Evolution*.

Tian, S., Bowen, L., Liu, B., Zeng, F., Xue, H., Erastova, V., et al. (2021). A Method for Automatic Shale Porosity Quantification Using an Edge-Threshold Automatic Processing (ETAP) Technique. *Fuel* 304, 121319. doi:10.1016/j.fuel.2021.121319

Tissot, B., Durand, B., Espitalie, J., and Combaz, A. (1974). Influence of Nature and Diagenesis of Organic Matter in Formation of Petroleum. *AAPG Bull.* 58 (3), 499–506. doi:10.1306/83d91425-16c7-11d7-8645000102c1865d

Walsh, I., Dymond, J., and Collier, R. (1988). Rates of Recycling of Biogenic Components of Settling Particles in the Ocean Derived from Sediment Trap Experiments. *Deep Sea Res. A. Oceanographic Res. Pap.* 35 (1), 43–58. doi:10.1016/0198-0149(88)90056-8

Wang, J., Zhang, C., Zheng, D., Song, W., and Ji, X. (2020). Stability Analysis of Roof in Goaf Considering Time Effect. *J. Min Strat Control. Eng.* 2 (1), 013011.

Wang, Y., Liu, L., Meng, J., Jiang, Z., Gao, Y., and Liu, S. (2014). Depositional Environment of Es4uand Es3lShales Based on Biomarkers from the Boxing Sag of Dongying Depression, East China. *Acta Geologica Sinica - English Edition* 88 (5), 1556–1564. doi:10.1111/1755-6724.12318

Wu, J., Jiang, Z. X., and Liang, C. (2017). Lithofacies Characteristics of fine Grained Sedimentary Rocks in the Upper Submember of Member 4 of Shahejie Formation, Dongying Sag and Their Relationship with Sedimentary Environment. *Acta Petrolei Sinica* 38 (10), 1110–1120.

Wu, Y., Tahmasebi, P., Lin, C., Zahid, M. A., Dong, C., Golab, A. N., et al. (2019). A Comprehensive Study on Geometric, Topological and Fractal Characterizations of Pore Systems in Low-Permeability Reservoirs Based on SEM, MICP, NMR, and X-ray CT Experiments. *Mar. Pet. Geology.* 103, 12–28. doi:10.1016/j.marpetgeo.2019.02.003

Wu, Y., Tahmasebi, P., Yu, H., Lin, C., Wu, H., and Dong, C. (2020). Pore-scale 3D Dynamic Modeling and Characterization of Shale Samples: Considering the Effects of thermal Maturation. *J. Geophys. Res. Solid Earth* 125 (1), e2019JB018309. doi:10.1029/2019jb018309

Yu, X., Bian, J. Q., and Liu, C. Y. (2022). Determination of Energy Release Parameters of Hydraulic Fracturing Roof Near Goaf Based on Surrounding

Rock Control of Dynamic Pressure Roadway. *J. Min. Strata Control. Eng.* 4, 013016.

Zeng, F., Dong, C., Lin, C., Tian, S., Wu, Y., Lin, J., et al. (2022). Pore Structure Characteristics of Reservoirs of Xihu Sag in East China Sea Shelf Basin Based on Dual Resolution X-ray Computed Tomography and Their Influence on Permeability. *Energy* 239, 122386. doi:10.1016/j.energy.2021.122386

Zeng, F., Dong, C., Lin, C., Wu, Y., Tian, S., Zhang, X., et al. (2021). Analyzing the Effects of Multi-Scale Pore Systems on Reservoir Properties-A Case Study on Xihu Depression, East China Sea Shelf Basin, China. *J. Pet. Sci. Eng.* 203, 108609. doi:10.1016/j.petrol.2021.108609

Zhang, K., Jia, C., Song, Y., Jiang, S., Jiang, Z., Wen, M., et al. (2020a). Analysis of Lower Cambrian Shale Gas Composition, Source and Accumulation Pattern in Different Tectonic Backgrounds: a Case Study of Weiyuan Block in the Upper Yangtze Region and Xiuwu Basin in the Lower Yangtze Region. *Fuel* 263, 115978. doi:10.1016/j.fuel.2019.115978

Zhang, K., Jiang, Z., Song, Y., Jia, C., Yuan, X., Wang, X., et al. (2020b). Quantitative Characterization for Pore Connectivity, Pore Wettability, and Shale Oil Mobility of Terrestrial Shale with Different Lithofacies--A Case Study of the Jurassic Lianggaoshan Formation in the Southeast Sichuan Basin of the Upper Yangtze Region in Southern China. *Front. Earth Sci.*, 312. doi:10.3389/feart.2022.864189

Zhang, K., Song, Y., Jia, C., Jiang, Z., Han, F., Wang, P., et al. (2022b). Formation Mechanism of the Sealing Capacity of the Roof and Floor Strata of marine Organic-Rich Shale and Shale Itself, and its Influence on the Characteristics of Shale Gas and Organic Matter Pore Development. *Mar. Pet. Geology.* 140, 105647. doi:10.1016/j.marpetgeo.2022.105647

Zhang, K., Song, Y., Jiang, Z., Xu, D., Li, L., Yuan, X., et al. (2022c). Quantitative Comparison of Genesis and Pore Structure Characteristics of Siliceous Minerals in Marine Shale with Different TOC Contents-A Case Study on the Shale of Lower Silurian Longmaxi Formation in Sichuan Basin, Southern China. *Front. Earth Sci.*, 437. doi:10.3389/feart.2022.887160

Zhang, K., Song, Y., Jiang, Z., Yuan, X., Wang, X., Han, F., et al. (2022d). Research on the Occurrence State of Methane Molecules in post-mature marine Shales-A Case Analysis of the Lower Silurian Longmaxi Formation Shales of the Upper Yangtze Region in Southern China. *Front. Earth Sci.*, 247.

Zhao, X., Li, Q., Jiang, Z., Zhang, R., and Li, H. (2014). Organic Geochemistry and Reservoir Characterization of the Organic Matter-Rich Calcilutite in the Shulu Sag, Bohai Bay Basin, North China. *Mar. Pet. Geology.* 51, 239–255. doi:10.1016/j.marpetgeo.2013.12.014

Zheng, R., and Liu, M. (1999). Study on Palaeosalinity of Chang-6 Oil Reservoir Set in Ordos Basin. *Oil Gas Geology.* 20 (1), 20–25.

Conflict of Interest: Author LJ was employed by Shengli Oilfield, SINOPEC. Author FG was employed by Liaohe Oilfield, CNPC.

The remaining authors declare that the research was conducted in the absence of any commercial or financial relationships that could be construed as a potential conflict of interest.